Ultrashort spatiotemporal optical solitons in waveguide arrays: The effect of combined linear and nonlinear couplings

Hervé Leblond[1] **and Dumitru Mihalache**[2]

[1] Laboratoire de Photonique d'Angers, EA 4464, LUNAM Université, Université d'Angers, 2 Boulevard Lavoisier, 49000 Angers, France

[2] Horia Hulubei National Institute for Physics and Nuclear Engineering, 30 Reactorului, Magurele-Bucharest, RO-077125, Romania

Abstract.

We investigate the propagation of Gaussian spatiotemporal inputs in arrays of parallel optical waveguides, assuming both linear and nonlinear non-dispersive coupling between adjacent guides. The numerical simulations employ a discrete version of the modified Korteweg-de Vries equation that adequately describe the propagation of few-cycle spatiotemporal solitons in coupled waveguide arrays. It is shown that depending on the numerical values of the key parameters of the spatiotemporal Gaussian input, the combined effect of linear and nonlinear couplings leads to either the diffraction and dispersion spreading effect or to the formation of different types of (2+1)-dimensional ultrashort spatiotemporal solitons such as one or many single-channel few-cycle solitons, and half-cycle (single-humped) ones.

Keywords: nonlinear optics, few-cycle optical pulses, discrete solitons, spatiotemporal solitons

Submitted to: *J. Phys. A: Math. Theor.*

1. Introduction

The problem of self-trapping of multidimensional localized structures in optical and matter-wave media and in other relevant physical settings has been investigated intensively over the past two decades, see for example the review papers [1, 2, 3, 4, 5, 6]. The stability of these multidimensional solitons is a key issue due to the presence of wave collapse that prevents the stable propagation in many physical settings. However, the use of arrays of evanescently coupled nonlinear waveguides has provided the adequate setting where the dispersion and/or diffraction of input optical wave packets can be controlled and engineered in a proper way, such that many kinds of *discrete optical solitons* can propagate stably, see for example Refs. [7, 8, 9]. After the pioneering work of Christodoulides and Joseph [10], published three decades ago, in which the two authors theoretically investigated the problem of discrete self-focusing in nonlinear arrays of coupled waveguides and the formation of one-dimensional (1D) discrete solitons, many theoretical and experimental works have investigated the combined discrete-continuous solitons in both two-dimensional (2D) and three-dimensional (3D) settings, see, for example, Refs. [11, 12, 13, 14, 15, 16, 17, 18, 19, 20, 21, 22, 23, 24, 25, 26, 27, 28, 29, 30]. We highlight here the works reporting the observation of discrete spatial solitons in optically induced nonlinear photonic lattices [23, 24, 25], the experimental generation of both 1D and 2D discrete surface solitons in waveguide arrays [26, 27], and the observation of 3D discrete-continuous X waves in photonic lattices [28]. The 3D discrete-continuous spatiotemporal solitons in 2D arrays of coupled waveguides have been observed by Minardi et al. [29], and the vortex light bullets that are discrete spatiotemporal solitons with embedded orbital angular momenta have been predicted theoretically in Refs. [31, 32] and experimentally evidenced by Eilenberger et al. [30]. On the experimental arena in the broad area of spatiotemporal optical solitons (alias light bullets) it is also worth mentioning the recent work by Lahav et al. [33] on the experimental realization of 3D spatiotemporal pulse-train solitons, which is based on utilizing a combination of slow saturable self-focusing nonlinearity and a fast self-phase modulation. On the theoretical arena, we mention a recent theoretical work by Veretenov et al. [34] predicting a new class of 3D topological dissipative optical solitons, termed "hula-hoop solitons", in homogeneous laser media with fast saturable absorption. Recently, Shtyrina et al. [35] have studied theoretically the problem of coexistence of collapse and the formation of stable spatiotemporal solitons in graded-index multimode optical fibres. Families of stable fundamental and dipole-mode spatiotemporal solitons were analysed in detail by using both analytical (variational) and numerical methods, see Ref. [35].

During the past decades a lot of studies have been devoted to the nonlinear optical pulse propagation in the few-cycle regime in a series of physical settings. Some of these works were based on the slowly varying envelope approximation (SVEA) and different types of generalizations of the generic nonlinear Schrödinger (NLS) equation; see, for example, the study of Brabec and Krausz [36] on the nonlinear pulse propagation in the

single-cycle regime and that of Amiranashvili et al. [37] on a generalized NLS equation, which includes dispersion of the intensity-dependent group velocity. However, many theoretical approaches beyond the SVEA have been proposed during the past years. Here we only bring the readers' attention to the unidirectional pulse propagation model [38, 39], the Maxwell-Duffing description of ultrashort optical pulses in nonresonant media [40], and the Maxwell-Drude-Bloch model of few-cycle optical solitons [41]. The theoretical and experimental researches in the broad area of nonlinear optics of ultrashort light pulses including few-cycle optical solitons have been reviewed in a series of papers [42, 43, 44, 45]. The series of theoretical approaches beyond the SVEA (most of them being (1+1)-dimensional models) rely on generic nonlinear evolution models such as the modified Korteweg-de Vries (mKdV) [46], the short-pulse [47, 48, 49], the sine-Gordon (sG) [50], the double sG [51, 52], and the mKdV-sG [53, 54, 55] equations. We also refer to other relevant works in this area, see Refs. [56, 57, 58, 59, 60, 61, 62, 63].

In a recent work [64], using a non-SVEA model that is valid in the few-cycle regime, the generic equations accounting for the waveguide coupling between two adjacent optical waveguides have been introduced and studied by numerical methods. The non-SVEA model was based on the generalized Kadomtsev-Petviashvili equation and from this equation a set of two coupled mKdV equations was derived [64]. The analysis reported in Ref. [64] has been extended in Ref. [65], where it was investigated the stable propagation of few-cycle vector solitons of breather type, in two parallel optical waveguides, in the presence of linear non-dispersive coupling. The extensive numerical simulations were performed on a set of two coupled continuous mKdV equations [65]. Recently [66] we introduced and studied in detail the discrete version of the coupled continuous mKdV equations. Two kinds of such discrete-continuous spatiotemporal solitons, which are discrete solitons in the transverse direction, and few-cycle solitons in the longitudinal one, were put forward, namely breathing-type solitons and single-humped ones [66].

In the present work we study the formation of few-cycle spatiotemporal optical solitons in coupled waveguide arrays in the regime of combined linear and nonlinear couplings. The organization of this paper is as follows. In Sec. II we present the generic model describing the propagation of few-cycle spatiotemporal optical solitons in waveguide arrays, which is based on a discrete version, see Eq. (1), of coupled mKdV equations. We investigate both the continuous and the SVEA limits of Eq. 1. The continuous version of the coupled discrete mKdV equations is a generalized NLS-type equation that was not yet considered in the literature, to the best of our knowledge. We also study the modulation instability phenomenon described by the thus obtained generalized NLE equation (24). The detailed numerical study of the formation of different types of (2+1)-dimensional spatiotemporal solitons from Gaussian inputs is given in Sec. III. We consider four types of non-dispersive linear and nonlinear couplings: a) focusing linear coupling and defocusing nonlinear one, b) defocusing linear coupling and focusing nonlinear one, c) both types of couplings are focusing ones, and d) both types of couplings are defocusing ones. We also vary the key characteristics of initial

Gaussian optical waveform, namely the initial field amplitude and the initial width in the spatial transverse direction. Finally, Sec. IV concludes this paper.

2. The model

We consider a set of $2N+1$ parallel waveguides in a planar geometry, assuming both linear and nonlinear coupling between these waveguides. The normalized optical electric field u_n propagating in the nth waveguide satisfies the following discrete version of the mKdV equation [64]:

$$\begin{aligned}&\partial_z u_n + a\partial_t(u_n^3) + b\partial_t^3 u_n + c\partial_t\left(u_{n-1}+u_{n+1}\right)\\&+f\partial_t\left[3{u_n}^2\left(u_{n+1}+u_{n-1}\right)+u_{n+1}^3+u_{n-1}^3\right]=0,\end{aligned}\tag{1}$$

which holds for $-N \leqslant n \leqslant N$ (with the convention that u_{-N-1} and u_{N+1} are replaced with zero).

2.1. The Lagrangian

It is straightforwardly proved that the system of coupled mKdV-type equations (1) conserves the quantity

$$E=\sum_{n=-N}^{N}\int_{-\infty}^{\infty}u_n^2 dt,\tag{2}$$

in the sense that $\partial_z E = 0$. E is proportional to the optical intensity integrated over space and time, and hence we will refer to as the pulse energy below. Equation (1) derives from the Lagrangian density

$$\mathcal{L}=\sum_{n=-N}^{N}\mathcal{L}_n+\mathcal{L}_I.\tag{3}$$

Here the Lagrangian density corresponding to channel n is

$$\mathcal{L}_n=\frac{1}{2}\partial_t\varphi_n\partial_z\varphi_n+\frac{a}{4}\left(\partial_t\varphi_n\right)^4-\frac{b}{2}\left(\partial_t^2\varphi_n\right)^2,\tag{4}$$

where

$$u_n=\partial_t\varphi_n,\tag{5}$$

and the interaction between channels is taken into account by

$$\mathcal{L}_I=c\sum_{n=-N}^{N-1}\partial_t\varphi_n\partial_t\varphi_{n+1}+f\sum_{n=-N}^{N-1}\left[\partial_t\varphi_n\left(\partial_t\varphi_{n+1}\right)^3+\left(\partial_t\varphi_n\right)^3\partial_t\varphi_{n+1}\right].\tag{6}$$

Equation (1) also conserves the Hamiltonian $H=\int_{-\infty}^{\infty}\mathcal{H}dt$, where the Hamiltonian density is defined by

$$\mathcal{H}=\sum_{n=-N}^{N}\mathcal{H}_n+\mathcal{H}_I,\tag{7}$$

with

$$\mathcal{H}_n = \frac{a}{4}u_n^4 + \frac{b}{2}u_n\partial_t^2 u_n, \tag{8}$$

and

$$\mathcal{H}_I = \mathcal{L}_I = c\sum_{n=-N}^{N-1} u_n u_{n+1} + f\sum_{n=-N}^{N-1}\left(u_n u_{n+1}^3 + u_n^3 u_{n+1}\right). \tag{9}$$

2.2. The continuous limit of Eq. (1)

A continuous limit of (1) can be sought by introducing a transverse variable x and a formal interpolation function $u(x)$ so that $u_n = u(x_n)$ with $x_n = nh$, h being some transverse pitch. Using a Taylor expansion we show that

$$u_{n-1} + u_{n+1} = 2u + h^2\partial_x^2 u + O(h^4), \tag{10}$$

and

$$(u_{n-1})^3 + (u_{n+1})^3 = 2u^3 + h^2\partial_x^2 u^3 + O(h^4), \tag{11}$$

in which the right-hand-side part of the above equation is evaluated at $x = x_n$.

Using the approximation formulas (10) and (11) in Eq. (1), we get its continuous version as

$$\begin{aligned}&\partial_z u + (a+8f)\partial_t(u^3) + b\partial_t^3 u + 2c\partial_t u + h^2 c\partial_x^2\partial_t u\\ &+6h^2 f\partial_t\left[u^2\partial_x^2 u + u\left(\partial_x u\right)^2\right] = 0.\end{aligned} \tag{12}$$

Setting $a' = a + 8f$, $c' = h^2 c$, $f' = 6h^2 f$, and $t' = t - 2cz$, Eq. (12) reduces to

$$\partial_z u + a'\partial_{t'}\left(u^3\right) + b\partial_{t'}^3 u + c'\partial_x^2\partial_{t'} u + f'\partial_{t'}\left[u^2\partial_x^2 u + u\left(\partial_x u\right)^2\right] = 0. \tag{13}$$

Equation (13) derives from the Lagrangian density

$$\mathcal{L} = \frac{1}{2}\partial_t\varphi\partial_z\varphi + \frac{a'}{4}\left(\partial_t\varphi\right)^4 - \frac{b'}{2}\left(\partial_t^2\varphi\right)^2 - \frac{c'}{2}\left(\partial_x\partial_t\varphi\right)^2 - \frac{f'}{2}\left(\partial_t\varphi\right)^2\left(\partial_x\partial_t\varphi\right)^2, \tag{14}$$

where

$$u = \partial_t\varphi. \tag{15}$$

Equation (13) also conserves the Hamiltonian $H = \int\int \mathcal{H}dtdx$, where the Hamiltonian density is defined by

$$\mathcal{H} = \frac{a'}{4}u^4 + \frac{b'}{2}u\partial_t^2 u - \frac{c'}{2}\left(\partial_x u\right)^2 - \frac{f'}{2}u^2\left(\partial_x u\right)^2. \tag{16}$$

2.3. The SVEA limit of Eq. (1)

The SVEA limit is found by using the standard multiscale formalism [67]. We drop the primes in Eq. (13) to simplify notations. We expand u in both a power series of a small parameter ε and in a Fourier series of some fundamental phase $\varphi = kz - \omega t$ as

$$u = \varepsilon v e^{i\varphi} + cc + \sum_{n\geqslant 2,|p|<n}\varepsilon^n v_{n,p}e^{ip\varphi}, \tag{17}$$

in which the profiles $v = v_{1,1}$ and $v_{n,p}$ for $n \geqslant 2$ are functions of the slow variables $\xi = \varepsilon x$, $\tau = \varepsilon(t - wz)$ and $\zeta = \varepsilon^2 z$, $1/w$ being some speed to be determined. The derivation operators are changed as

$$\partial_x = \varepsilon\partial_\xi, \quad \partial_t = -ip\omega + \varepsilon\partial_\tau, \tag{18}$$

$$\partial_z = ipk - \varepsilon w\partial_\tau + \varepsilon^2\partial_\zeta. \tag{19}$$

Then the equation is solved, by Fourier component and order by order in ε. At leading order ε^1, and for the fundamental Fourier component $p = 1$, it yields the equation

$$ipkv = -b' \times (-ip\omega)^3 v, \tag{20}$$

which provides the linear dispersion relation of Eq. (13) as

$$k = -b'\omega^3. \tag{21}$$

At order ε^2 and for the Fourier harmonic p, the equation is

$$ipkv_{2,p} - w\partial_\tau v_{1,p} = -b' \left[(-ip\omega)^3 v_{2,p} + 3 \times (-ip\omega)^2 \partial_\tau v_{1,p}\right], \tag{22}$$

which, using (21), reduces to $v_{2,p} = 0$ for $p \neq \pm 1$ and gives $w = -3b'\omega^2$ for $p = \pm 1$. It is checked that, as expected, $w = dk/d\omega$, where the function $k(\omega)$ is defined by (21).

The equation for the fundamental Fourier component at order ε^3 is

$$\begin{aligned} &ikv_{3,1} - w\partial_\tau v_{2,1} + \partial_\zeta v_{1,1} = a'i\omega \sum_{l+m+n=1} v_{1,l} v_{1,m} v_{1,n} \\ &-b' \left[i\omega^3 v_{3,1} - 3\omega^2 \partial_\tau v_{2,1} - 3i\omega\partial_\tau^2 v_{1,1}\right] + c'i\omega\partial_\xi^2 v_{1,1} \\ &+f'i\omega \left[\sum_{l+m+n=1} v_{1,l} v_{1,m} \partial_\xi^2 v_{1,n} + \sum_{l+m+n=1} v_{1,l} \left(\partial_\xi v_{1,m}\right) \left(\partial_\xi v_{1,n}\right)\right]. \end{aligned} \tag{23}$$

The terms involving $v_{3,1}$ vanish using (21), and the terms involving $v_{2,1}$ vanish using the expression of w. After explicit computation of the nonlinear terms, the nonlinear evolution equation for $v = v_{1,1}$ becomes

$$\begin{aligned} &i\partial_\zeta v + Av|v|^2 + B\partial_\tau^2 v + C\partial_\xi^2 v \\ &+F\left[v^2\partial_\xi^2 v^* + 2|v|^2\partial_\xi^2 v + 2\left|\partial_\xi v\right|^2 v + \left(\partial_\xi v\right)^2 v^*\right] = 0, \end{aligned} \tag{24}$$

where we have set $A = 3a'\omega$, $B = 3b'\omega$, $C = c'\omega$, and $F = f'\omega$.

It is seen that, in the case of a purely linear coupling, i.e. when $f = 0$ (and hence $F = 0$), Eq. (24) is the standard two-dimensional cubic nonlinear Schrödinger equation. However, it appreciably differs from the standard model in the case of nonlinear coupling between parallel optical waveguides ($f \neq 0$).

Equation (24) derives from the Lagrangian density

$$\begin{aligned} \mathcal{L} = &\frac{i}{4}\left(v^*\partial_\zeta v - v\partial_\zeta v^*\right) + \frac{A}{4}\left|v\right|^4 - \frac{B}{2}\left|\partial_\tau v\right|^2 - \frac{C}{2}\left|\partial_\xi v\right|^2 \\ &- \frac{F}{4}\left[\left(\partial_\xi \left|v\right|^2\right)^2 + 2\left|v\right|^2\left|\partial_\xi v\right|^2\right] \end{aligned} \tag{25}$$

according to

$$\partial_\zeta \frac{\partial\mathcal{L}}{\partial(\partial_\zeta v^*)} + \partial_\tau \frac{\partial\mathcal{L}}{\partial(\partial_\tau v^*)} + \partial_\xi \frac{\partial\mathcal{L}}{\partial(\partial_\xi v^*)} = \frac{\partial\mathcal{L}}{\partial v^*}. \tag{26}$$

We see that Eq. (24) also conserves the Hamiltonian $H = \int\int \mathcal{H} dtdx$, where the Hamiltonian density is defined by

$$\mathcal{H} = \frac{A}{4}|v|^4 - \frac{B}{2}|\partial_\tau v|^2 - \frac{C}{2}|\partial_\xi v|^2 - \frac{F}{4}\left[\left(\partial_\xi |v|^2\right)^2 + 2|v|^2|\partial_\xi v|^2\right]. \quad (27)$$

2.4. The study of modulation instability of Eq. (24)

Since Eq. (24) appreciably differs from standard nonlinear models, it is worth performing some analysis in order to have an insight on its behaviour. We will only consider the transverse evolution, i.e., we drop the variable τ in Eq. (24). It admits the constant solution $u_0 = \mathcal{A}e^{iK\zeta}$ provided that $K = A\mathcal{A}^2$ ($\mathcal{A}$ being an arbitrary real constant). We study the modulation instability of u_0 [68, 69]. Therefore we set $u = u_0(1+g)$, where the term $g = g(\zeta, \xi)$ is very small with respect to one. The equation satisfied by g is

$$i\partial_\zeta g + A\mathcal{A}^2(g + g^*) + C\partial_\xi^2 g + F\mathcal{A}^2\left(\partial_\xi^2 g^* + 2\partial_\xi^2 g\right) = 0. \quad (28)$$

We seek for solutions of the form $g = g_1 e^{\Phi} + g_2 e^{\Phi^*}$ with $\Phi = \lambda\zeta - i\omega\xi$. Equation (28) then reduces to

$$(i\lambda + M + P)g_1 + Pg_2^* = 0, \quad (29)$$

$$Pg_1 + (-i\lambda + M + P)g_2^* = 0, \quad (30)$$

with

$$M = -\omega^2\left(C + F\mathcal{A}^2\right), \quad P = \left(A - \omega^2 F\right)\mathcal{A}^2. \quad (31)$$

The nonzero solutions f exist if

$$\lambda^2 = \omega^2\left(C + F\mathcal{A}^2\right)\left(2A\mathcal{A}^2 - \omega^2 C - 3\omega^2 F\mathcal{A}^2\right). \quad (32)$$

Recall that the modulation instability occurs if one solution for λ has a nonzero positive real part, hence here if $\lambda^2 > 0$. Assuming that $A > 0$ for simplicity, we obtain:

- If $C > 0$ and $F > 0$, instability occurs for $\omega < \omega_0$, with $\omega_0^2 = 2A\mathcal{A}^2/(C + 3F\mathcal{A}^2)$.
- If $C < 0$ and $F < 0$, instability never occurs.
- If $C > 0$ and $F < 0$, instability occurs for $\omega < \omega_0$ if $-F\mathcal{A}^2 < C/3$; for any ω if $C/3 < -F\mathcal{A}^2 < C$; and does not occur if $-F\mathcal{A}^2 > C$.
- If $C < 0$ and $F > 0$, instability does not occur if $F\mathcal{A}^2 < -C/3$; it occurs for any $\omega > \omega_0$ if $-C/3 < F\mathcal{A}^2 < -C$; and it occurs for $\omega < \omega_0$ if $F\mathcal{A}^2 > -C$.

In accordance with Benjamin and Feir's analysis [68], we expect soliton formation as modulation instability occurs for $\omega < \omega_0$, and stability of plane wave, corresponding to the spreading out of pulses, when no instability of this kind occurs. A third situation can be found in the present case, as arbitrary high frequencies are subject to the instability.

However, other situations as bistability between continuous wave and solitons might occur, and the existence of solitons must be investigated numerically. We solve numerically Eq. (24) in the Fourier space, using a standard 4th-order Runge-Kutta scheme, the nonlinear terms being computed by one inverse and one inverse and one

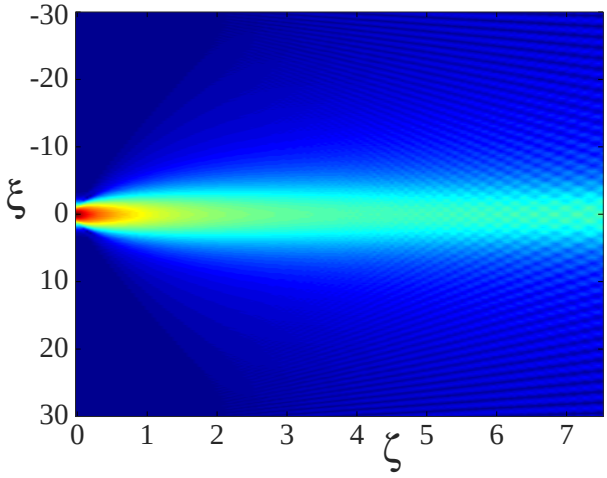

Figure 1. Example of a soliton solution to Eq. (24), for $A = C = F = 1$, and initial peak amplitude $A_0 = 1.58$ and area $A_0 l_x = 2.5$.

direct fast Fourier transform at each substep of the evolution scheme. We use initial data of the form

$$v = A_0 e^{-\xi^2/l_x^2}. \tag{33}$$

The normalized Kerr coefficient in Eq. 24 is set to $A = 1$ in this work. The energy and Hamiltonian of the pulse are computed and the step in the propagation variable ζ is decreased until both quantities are conserved.

The transform

$$v \longrightarrow v\sqrt{\left|\frac{F}{C}\right|}, \quad \zeta \longrightarrow \zeta\left|\frac{AC}{F}\right|, \quad \tau \longrightarrow \tau\sqrt{\left|\frac{AC}{BF}\right|}, \quad \xi \longrightarrow \xi\sqrt{\left|\frac{A}{F}\right|}, \tag{34}$$

changes the coefficient A in Eq. (24)into 1 and B, C, F into ± 1. As a consequence we restrict the computation to these values of A, C and F without loss of generality.

2.4.1. The case $C = +1$ and $F = +1$. According to the analysis of the modulation instability phenomenon, we can expect soliton formation in this case. We consider a set of values of A_0 ranging from 0.025 to 2.5, and $l_x = 2.5/A_0$. Although the numerical convergence is difficult to obtain, soliton formation is observed in every case, see Fig. 1 (the interference pattern that can be seen at the end of the computation is only due to the periodic boundary conditions used in the numerical scheme). Obviously, linear diffraction occurs for smaller values of the pulse area $l_x A_0$.

2.4.2. The case $C = -1$ and $F = -1$. According to the modulation instability analysis, no soliton formation is expected. we consider a set of values of A_0 ranging from about 0.35 to 1.35, with l_x yielding pulse areas ranging from 2 to 5.8. Diffraction always occurs. It is noted that the beam spreads out much faster for higher amplitudes: it is the nonlinear diffraction effect (see Fig. 2).

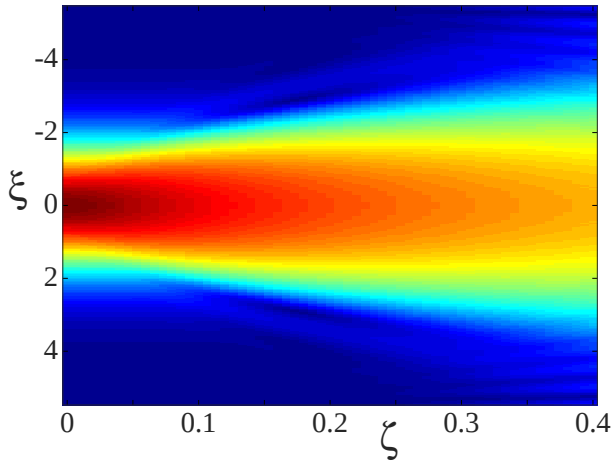

Figure 2. Example of nonlinear diffraction according to Eq. (24), for $A = 1$, $C = F = -1$, and initial peak amplitude $A_0 = 1.643$ and area $A_0 l_x = 3$.

2.4.3. The case $C = +1$ and $F = -1$. In the preceding analysis we found that the modulation instability with arbitrary high frequency occurs in the domain where $1/3 < \mathcal{A}^2 < 1$. This results on a strong instability of the solution, as soon as the local amplitude exceeds $1/\sqrt{3} \simeq 0.577$. However, if we consider the Gaussian pulse (33), with $A_0 < 1/\sqrt{3}$, this instability should not arise, as long as the peak amplitude does not increase. According to the modulation instability analysis, we can expect in this case soliton formation. In fact, it is found that soliton forms for $A_0 \leqslant A_{0th}$, where A_{0th} can take values about 0.39, 0.43, or 0.5 for $l_x = 5.2$, 4 or 2, respectively. Self-focusing indeed occurs for such values of the parameters, and the high-frequency modulation instability develops as soon as the peak amplitude exceeds $1/\sqrt{3}$, which is checked numerically. However, the high-frequency modulation instability is strongly affected by the frequency cut-off due to discretization, and consequently cannot be analysed numerically with a reasonable reliability. When the peak amplitude A_0 exceeds the second threshold value, $A_0 \geqslant 1$, above which no modulation instability occurs any more in the case of a plane wave, the high-frequency instability still occurs, however, not at the top of the pulse, but on its lateral sides (see Fig. 3. Here the energy fails to be conserved by the numeric scheme about $z = 0.026$). Here also intrinsic limitations of numerics prevent further analysis.

2.4.4. The case $C = -1$ and $F = +1$. The modulation instability with arbitrary high frequency occurs here also in the domain where $1/3 < \mathcal{A}^2 < 1$. However, below this domain, the spreading out of the beam by diffraction can be expected, while above it, the modulation instability within some finite range of values of ω, which usually indicates the possibility of soliton formation, occurs. We consider a set of input of the form (33) with values of A_0 ranging from 0.2 to 0.77 and $A_0 l_x$ ranging from 2 to 4. We observe diffraction for $A_0 \leqslant 0.573$, and high-frequency instability for $A_0 \geqslant 0.574$: the numerically observed threshold is very close to that predicted analytically, $1/\sqrt{3} \simeq 0.577$. Indeed, since the

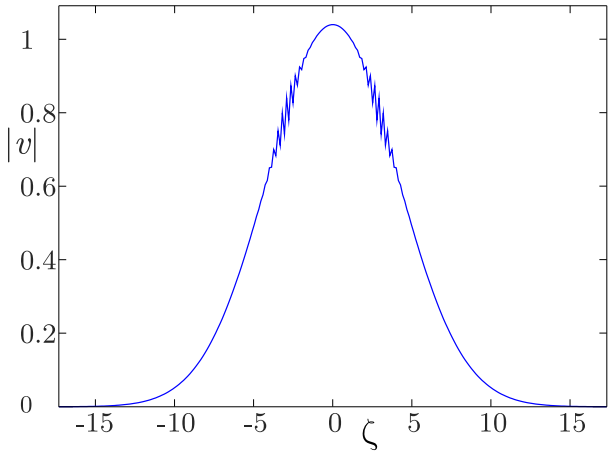

Figure 3. Example of high-frequency instability according to Eq. (24), for $A = 1$, $C = 1$, $F = -1$, initial peak amplitude $A_0 = 1.04$ and pulse area $A_0 l_x = 6$. Here the amplitude profile at $\zeta = 0.087$ is shown.

beam is spread out by diffraction, its peak amplitude is maximal at the input. For a value of A_0 larger than the second threshold value, 1, the pulse is destroyed after a short propagation distance by the growth of high-frequency perturbations on its lateral sides, in a way comparable to what was observed for $C = +1$ and $F = -1$ (see Fig. 3).

As a conclusion, positive values of F correspond to a focusing effect, and negative values to a defocusing one. When both C and F have the same sign, the effect is merely enhanced. When C and F have opposite signs, the term in F does not modify qualitatively the behaviour unless the amplitude is high enough. Then a high frequency instability occurs. In the discrete situation, this instability might be ineffective. In the continuous situation, it prevents further numerical analysis. However, the modulation instability with finite bandwidth, which is usually the indication that solitons may form, occurs for positive F, when nonlinear coupling dominates, and does not occur for negative F, except when the focusing linear coupling dominates, which confirms that the positive nonlinear coupling is focusing and the negative one is defocusing.

3. Formation of (2+1)-dimensional spatiotemporal solitons from Gaussian inputs

We solve Eqs. (1) in the Fourier space, using a standard 4th-order Runge-Kutta scheme, the nonlinear terms being computed by one inverse and one inverse and one direct fast Fourier transform at each substep of the evolution scheme. We use initial data of the form

$$u_n(z = 0, t) = A_0 \sin(\omega t) e^{-t^2/\tau^2} e^{-n^2/l_x^2}. \tag{35}$$

We denote by τ the half duration at $1/e$, which is related to the full width at half maximum Δt, according to $\tau = \Delta t/\sqrt{2 \ln 2}$; We fix the normalized angular frequency to $\omega = 0.6\pi$. This way, if a wavelength in vacuum of 1μm is assumed, Δt becomes the

pulse duration expressed in femtoseconds. If none of the quantities a, b and c vanishes, the transform

$$u_n \longrightarrow u_n\sqrt{\left|\frac{a}{c}\right|}, \quad z \longrightarrow z\sqrt{\left|\frac{c^3}{b}\right|}\mathrm{sgn}(a), \quad t \longrightarrow t\sqrt{\left|\frac{c}{b}\right|}, \quad f \longrightarrow \frac{f}{a}, \quad (36)$$

changes the coefficients a of Eq. (1) to 1 and b and c to ± 1. Hence we can restrict to these values without loss of generality.

3.1. The case $c > 0$, $f < 0$.

When $f < 0$ and $c > 0$, the nonlinear coupling is defocusing, and the linear coupling is focusing.

3.1.1. Varying nonlinear coupling f We fix $c = 1$, $A_0 = 2$, $\Delta t_0 = 4$, $l_x = 3$, and vary the strength of the negative nonlinear coupling coefficient f. When it is weak enough ($f \geqslant -0.14$), focusing occurs and a soliton forms, when it is larger ($f \leqslant -0.15$), the nonlinear coupling destroys the structure.

3.1.2. Varying initial amplitude A_0 In the same way, we fix $c = 1$, $f = -0.1$, $\Delta t_0 = 4$, $l_x = 3$, and vary A_0. As A_0 increases, the main soliton becomes narrower and taller, and increasing number of solitons may be excited, however, there is no qualitative change in the behaviour. We see here that the balance between focusing linear coupling and defocusing nonlinear coupling is not appreciably modified by changing the initial amplitude.

3.1.3. Varying initial width l_x We fix $c = 1$, $f = -0.1$, $A_0 = 2$, $\Delta t_0 = 4$, and vary l_x from 1 to 4. In all cases, self-focusing occurs and a single-channel soliton is formed. For $l_x = 4$, the spatial focusing is fast, and the temporal reshaping of the pulse occurs afterwards only. It leads to the formation of two solitons in the central channel, one of which turns into a stable spatiotemporal soliton, and the other is spread out by diffraction (see Fig. 4).

3.2. The case $c < 0$, $f > 0$.

We consider the other configuration where nonlinear and linear couplings are antagonists, i.e. a defocusing linear coupling and a focusing nonlinear one.

3.2.1. Varying nonlinear coupling f We fix $c = -1$, $A_0 = 2$, $\Delta t_0 = 4$, $l_x = 3$, and vary f. As expected, a soliton forms if f is large enough ($f \geqslant 0.17$) and the pulse diffracts if f is smaller than a certain value ($f \leqslant 0.16$).

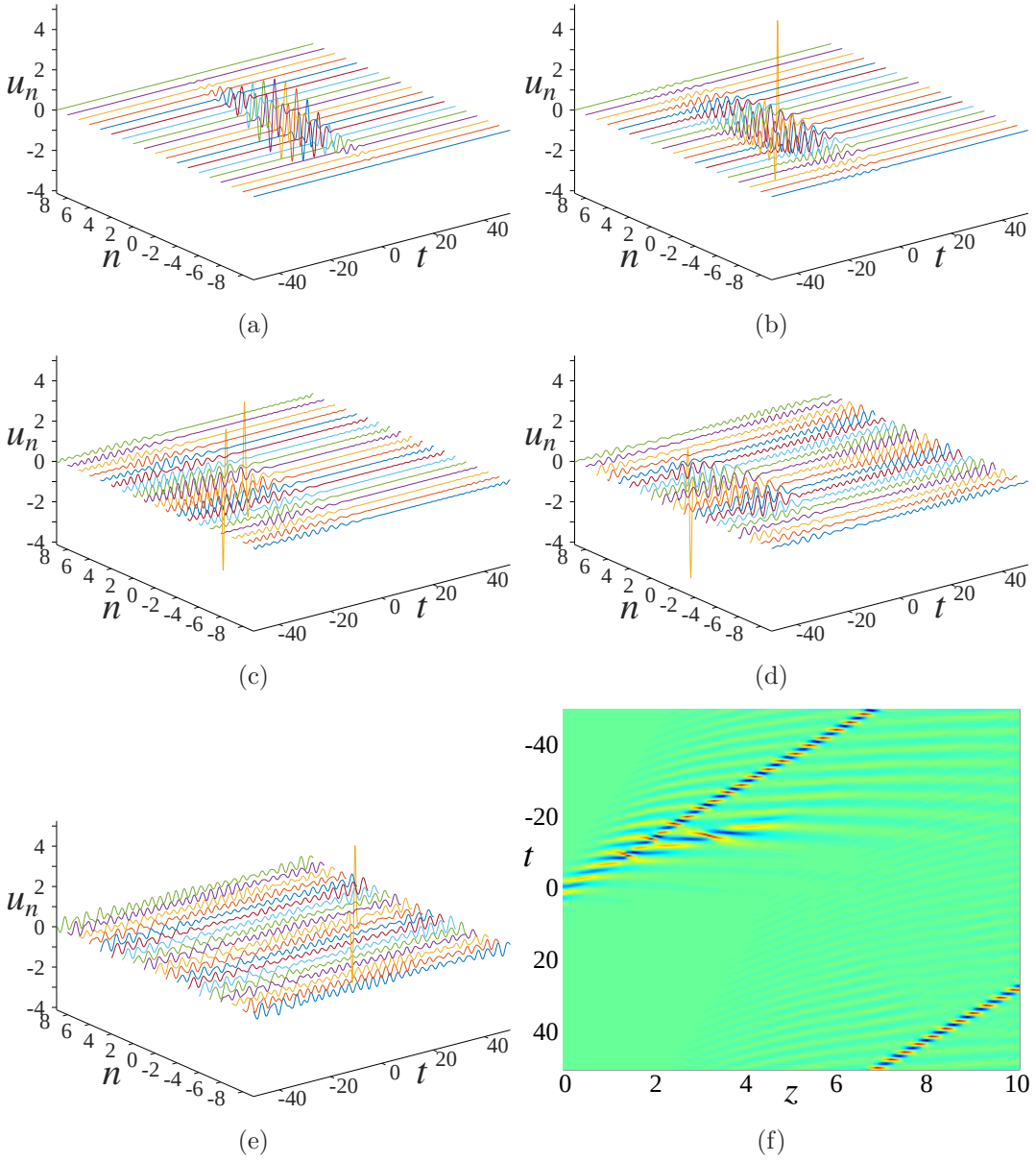

Figure 4. Formation of a single-channel soliton from a wide Gaussian input. Parameters are $c = 1$, $f = -0.1$, $A_0 = 2$, $\Delta t_0 = 4$, and $l_x = 4$. (a-e) show the temporal profile in all channels at several specific stages of the evolution: (a) $z = 0$, (b) $z = 1.4$, (c) $z = 3.1$, (d) $z = 5.9$, (e) $z = 10$. (f) shows the evolution of the temporal profile u_0 in the centre channel.

3.2.2. Varying initial amplitude A_0 In the same way, we fix $c = -1$, $f = 0.1$, $\Delta t_0 = 4$, $l_x = 3$, and vary A_0. As expected, a soliton forms if A_0 is high enough ($A_0 \geqslant 2.4$), while diffraction occurs if A_0 is smaller than a certain value ($A_0 \leqslant 2.3$). The contrast with the case where $c > 0$, $f < 0$ can be explained naturally. Here, as the amplitude decreases, the balance between nonlinear and linear couplings becomes more and more favourable to the defocusing coupling, and at the same time the diffraction is more efficient, so that solitons cannot form any more. In contrast, when $c > 0$, $f < 0$, the balance between

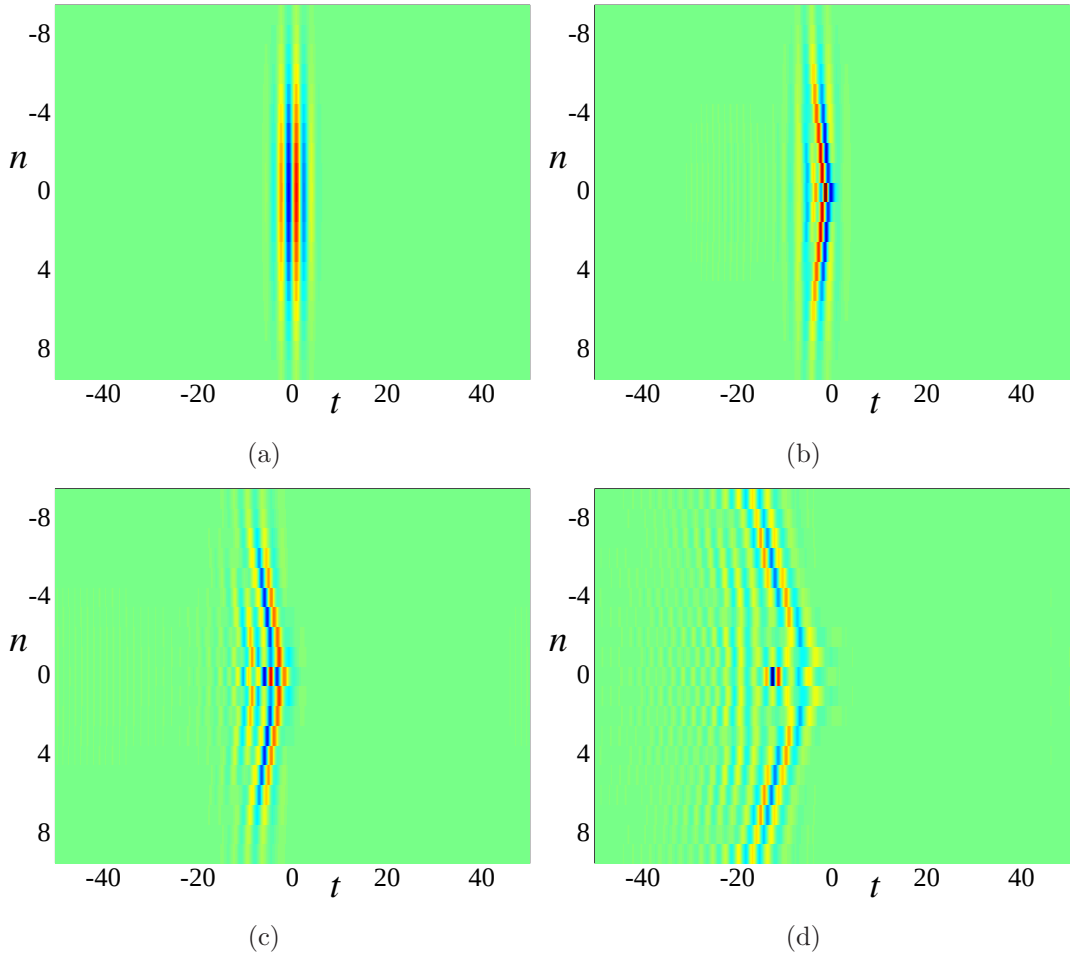

Figure 5. Formation of a single-channel soliton from a wide Gaussian input. Parameters are $c = -1$, $f = 0.1$, $A_0 = 2.2$, $\Delta t_0 = 4$, and $l_x = 6$. The four panels show the spatiotemporal pulse shape at several specific stages of the evolution: (a) $z = 0$, (b) $z = 0.3$, (c) $z = 0.6$, (d) $z = 1.35$.

nonlinear and linear couplings favours the focusing coupling for low amplitudes, but then the nonlinear effect becomes weaker with respect to the diffraction. As a result, the balance between diffraction and nonlinear focusing changes little, and the soliton formation is less dependent of the amplitude than in the situation considered in the present paragraph.

3.2.3. Varying initial width l_x We fix $c = -1$, $f = 0.1$, $A_0 = 2$, $\Delta t_0 = 4$, and vary l_x. A soliton forms if l_x is large enough ($l_x \geqslant 6$), and the pulse diffracts in the opposite case ($l_x \leqslant 5.9$). Of course, we chose values so that diffraction occurs for small l_x, using e.g. a higher amplitude we could have a soliton for any meaningful l_x (say, $l_x \gtrsim 1$). The result is that the transverse focusing due to nonlinear coupling is driven by the peak power rather than by the peak intensity. For $l_x = 6$, however, an important part of the pulse energy is not caught in the soliton but is diffracted, see Fig. 5.

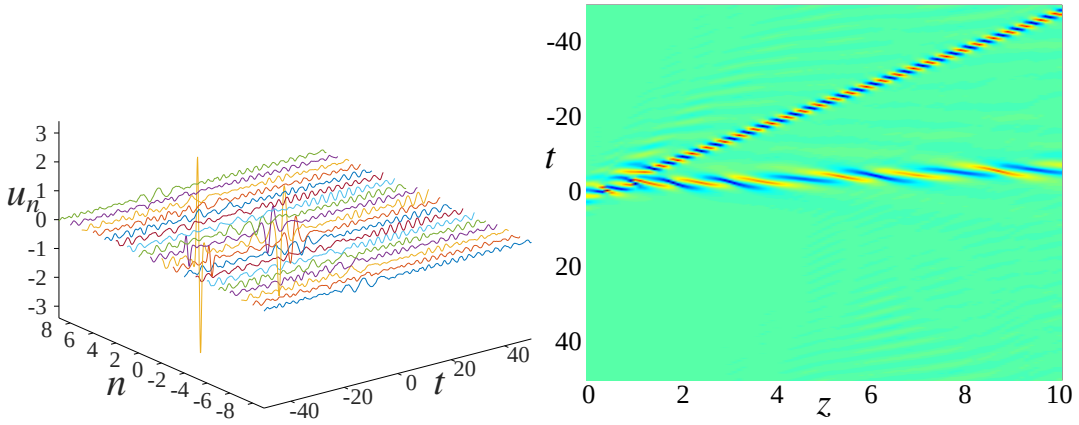

Figure 6. Formation of two single-channel solitons from a Gaussian input. Parameters are $c = 1$, $f = 0.05$, $A_0 = 2$, $\Delta t_0 = 4$, and $l_x = 3$. (a) the spatio-temporal profile at $z = 7.5$. (b) the evolution of the temporal profile u_0 in the centre channel.

3.3. The case $c > 0$, $f > 0$

We assume now that both coupling terms are focusing ones.

3.3.1. Varying nonlinear coupling f We fix $c = 1$, $A_0 = 1$, $\Delta t_0 = 4$, $l_x = 3$, and vary f. A smaller amplitude as before must be considered, because the nonlinear effects work together instead of being competing ones. For low f ($f \leqslant 0.11$), diffraction occurs, while for high f ($f > 0.12$) a soliton forms. This is not surprising: the soliton forms when the nonlinear coupling increases.

For large values of the nonlinear coupling, e.g., for $f = 0.03$ or 0.04, a second soliton may form and can be unstable due to diffraction as seen in the case $c > 0$, $f < 0$ (Fig. 4). For a even higher nonlinear coupling, the second soliton can be stable (see Fig. 6, for $f = 0.05$).

3.3.2. Varying initial amplitude A_0 We fix $c = 1$, $f = 0.1$, $\Delta t_0 = 4$, $l_x = 3$, and vary A_0. As expected, soliton forms for high A_0 ($A_0 \geqslant 1.1$), and diffraction occurs for low ones ($A_0 \leqslant 1$).

3.3.3. Varying initial width l_x We fix $c = 1$, $f = 0.1$, $A_0 = 1$, $\Delta t_0 = 4$, and vary l_x. Diffraction occurs for $l_x \leqslant 3.1$, soliton forms for $l_x \geqslant 3.2$. Again, the power drives the soliton formation, and not the amplitude only.

3.4. The case $c < 0$, $f < 0$

In this case both coupling terms are expected to be defocusing.

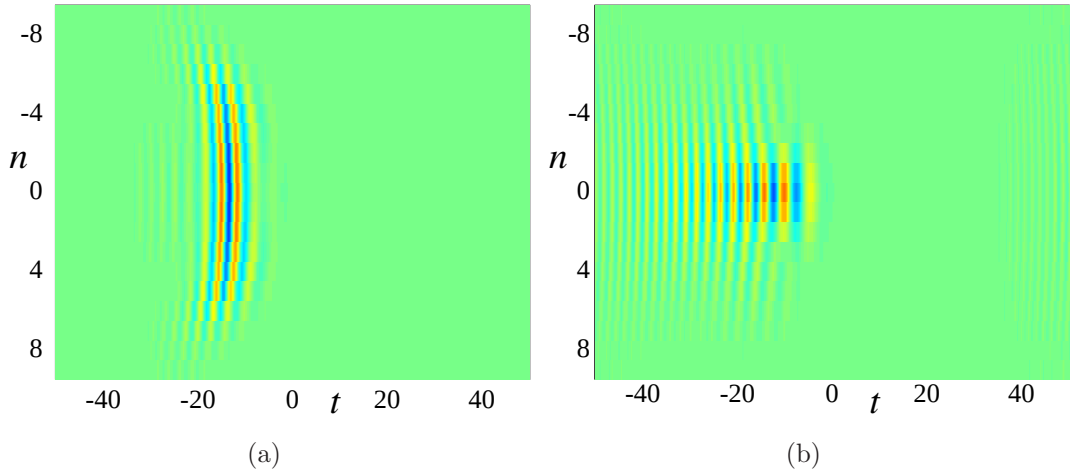

Figure 7. The spatiotemporal pulse profile at $z = 1.2$ showing the diffraction-dispersion of an initial Gaussian input. The initial spatiotemporal pulse profile is identical to that shown in Fig. 9c. (a) $c = -1$, $f = -0.05$; (b) $c = -1$, $f = -0.4$. The other parameters are: $A_0 = 2$, $\Delta t_0 = 4$, and $l_x = 3$.

3.4.1. Varying nonlinear coupling f We fix $c = -1$, $A_0 = 2$, $\Delta t_0 = 4$, $l_x = 3$, and vary f from -0.03 to -2. No sharp transition occurs, but while diffraction dominates for small $|f|$, it is overcome by dispersion for large $|f|$. Strong dispersion may occur, even before any diffraction. And soliton never forms, obviously. For small $|f|$, diffraction dominates and dispersion is weak (Fig. 7a), while for large $|f|$, dispersion largely dominates and diffraction is appreciably smaller (Fig. 7b).

3.4.2. Varying initial amplitude A_0 We set $c = -1$, $f = -0.1$, $\Delta t_0 = 4$, $l_x = 3$, and vary A_0 from 2.5 to 6. For small and moderate amplitudes, $A_0 \leqslant 4.4$, diffraction occurs. For large amplitudes, $A_0 \geqslant 4.5$, the initial pulse decays into two or more very short single-channel solitons, in addition to a lot of radiation. They are not localized in the centre channel but are symmetrically disposed on either side of it. A surprising observation is made for a very large amplitude ($A_0 = 6$): a set of solitons of a type that totally differs from the previous one is formed. They are *half-cycle, single-humped pulses*, with a nonlinear velocity of the opposite sign to the breather solitons (see Fig. 8).

3.5. The case $c = 0$, $f < 0$

The surprising behaviour of the negative nonlinear coupling ($f < 0$) rises the question: what happens in the case of vanishing linear coupling? We thus set $c = 0$, $f = -0.1$, $\Delta t_0 = 4$, and $l_x = 3$, and consider several values of A_0 ranging from 1 to 3. It is found that for small amplitudes, $A_0 \leq 1.8$, the dispersion phenomenon occurs, and that several single-channel breathing solitons are formed for $A_0 \geq 1.9$. More precisely, the initial pulse breaks into a set of wave packets, several of which turn into solitons (see Fig. 9).

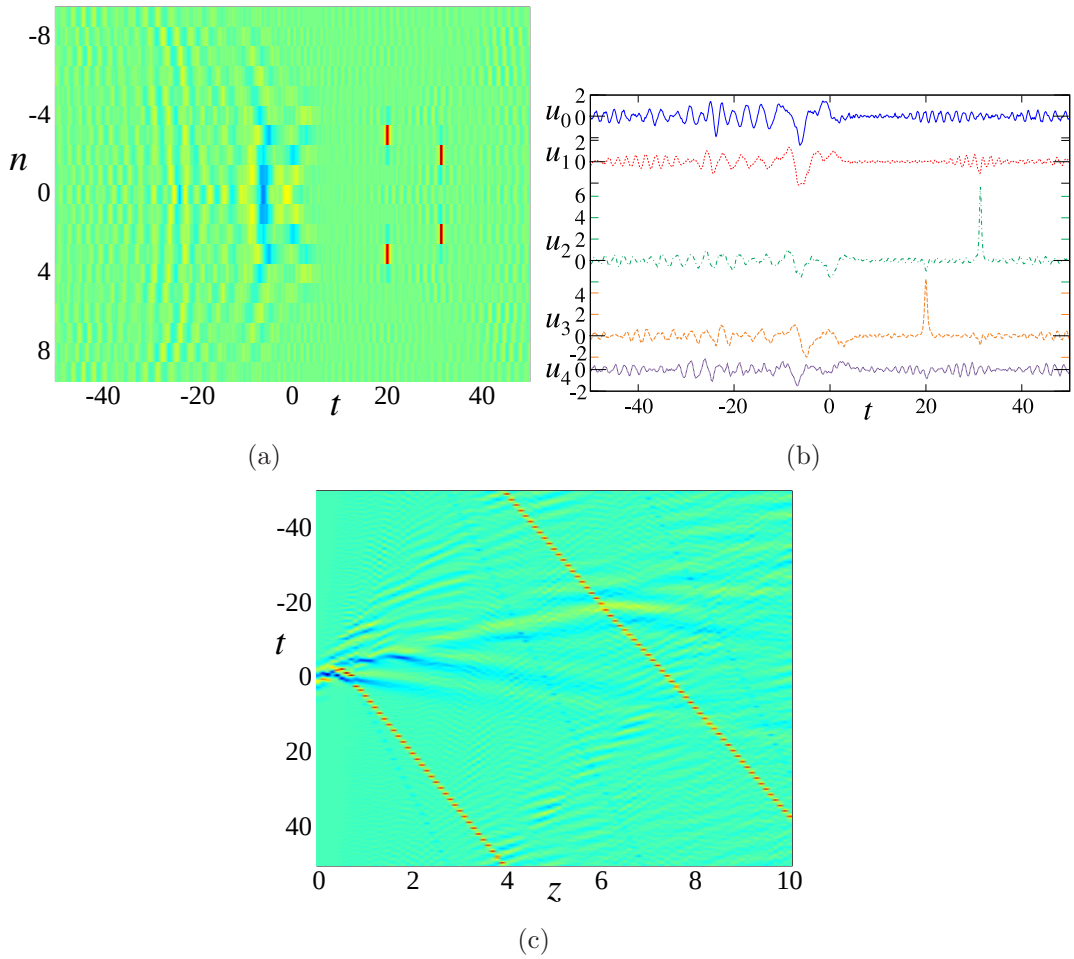

Figure 8. Formation of half-cycle, single-humped solitons from of a Gaussian input. The parameters are $c = -1$, $f = -0.1$, $A_0 = 6$, $\Delta t_0 = 4$, and $l_x = 3$. (a) the spatiotemporal pulse profile after its splitting, at $z = 2$. (b) the temporal profile at $z = 2$. The blue (solid), red (short dashing), green (dashed-dotted), orange (long dashing) and purple (dotted) lines correspond respectively to $n = 0$, 1, 2, 3 and 4. (c) the evolution of the temporal profile u_3 in a channel where a single-humped soliton forms and propagates ($n = 3$).

4. Conclusions

In this paper we have explored the behaviour of input few-cycle pulses in arrays of coupled waveguides, in the case where the nonlinear coupling evidenced in [64] cannot be neglected. The continuous limit of the model investigated in this work, within the SVEA, strongly differs from the standard NLS equation; see the generalized NLS-type equation (24). The modulation instability analysis of the continuous model (24) showed the possibility of soliton formation, but also the existence, at least from the purely mathematical point of view, of an irrecoverable high frequency instability.

In the corresponding discrete model, the nonlinear coupling strongly modifies the conditions of soliton formation with respect to the more usual linear coupling. In the case were linear coupling yields to soliton formation, a strong enough defocusing

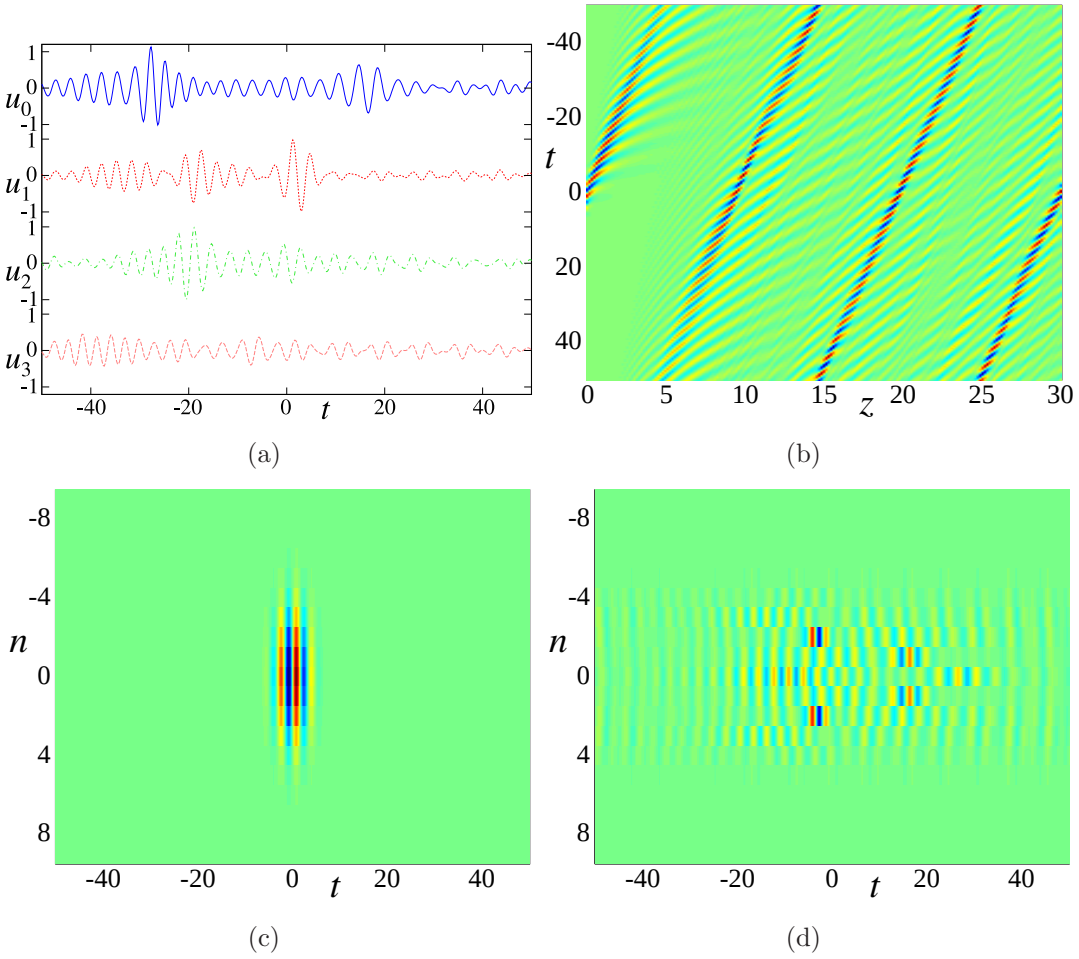

Figure 9. Splitting of a Gaussian input into a set of single-channel solitons. Parameters are $c = 0$, $f = -0.1$, $A_0 = 2.2$, $\Delta t_0 = 4$, and $l_x = 3$. (a) the temporal profile at $z = 11.4$. The blue (solid), red (short dashing), green (dashed-dotted), and orange (long dashing) lines correspond to $n = 0$, 1, 2, and 3, respectively. (b) the evolution of the temporal profile u_2 in a channel where a soliton forms and propagates. (c) the initial spatiotemporal pulse profile. (d) the spatiotemporal pulse profile after its splitting, at $z = 9.75$.

nonlinear coupling can destroy the soliton structure. Inversely, a strong enough focusing nonlinear coupling can overcome the diffraction induced by the defocusing linear one. Further, even the negative nonlinear coupling, which is expected to be a defocusing one according to the analysis of the SVEA limit, can lead to soliton formation at large input amplitudes. Although the solitons are always localized transversely in a single channel, more complex behaviours can occur in this case, leading to the decay of a wave packet into a set of single-channel solitons. But none of these solitons forms in the channel where the initial pulse was launched. This behaviour indicates some analogy with a filamentation phenomenon, but in the spatiotemporal domain. The whole analysis clearly shows that the study of wave coupling when few-cycle pulses are inputted in waveguide arrays cannot be restricted to the linear coupling case.

Finally we note that in [64] there were also identified coupling terms due to the dispersion effects, an issue that deserves a separate study. The investigation of propagation of few-cycle pulses in multidimensional structures, with linear and nonlinear couplings and the especially interesting issue whether the few-cycle pulses can carry vorticity as longer pulses can will be reported elsewhere.

[1] B. A. Malomed, D. Mihalache, F. Wise, and L. Torner, Spatiotemporal optical solitons, J. Opt. B.: Quantum Semiclass. Opt. **7**, R53 (2005).
[2] D. Mihalache, Multidimensional localized structures in optics and Bose-Einstein condensates: A selection of recent studies, Rom. J. Phys. **59**, 295 (2014).
[3] V. S. Bagnato, D. J. Frantzeskakis, P. G. Kevrekidis, B. A. Malomed, and D. Mihalache, Bose-Einstein condensation: Twenty years after, Rom. Rep. Phys. **67**, 5 (2015).
[4] B. Malomed, L. Torner, F. Wise, and D. Mihalache, On multidimensional solitons and their legacy in contemporary atomic, molecular and optical physics, J. Phys. B: At. Mol. Opt. Phys. **49**, 170502 (2016).
[5] B. A. Malomed, Multidimensional solitons: Well-established results and novel findings, Eur. Phys. J. Special Topics **225**, 2507 (2016).
[6] D. Mihalache, Multidimensional localized structures in optical and matter-wave media: A topical survey of recent literature, Rom. Rep. Phys. **69**, 403 (2017).
[7] D. N. Christodoulides, F. Lederer, and Y. Silberberg, Discretizing light behaviour in linear and nonlinear waveguide lattices, Nature (London) **424**, 817 (2003).
[8] F. Lederer, G. I. Stegeman, D. N. Christodoulides, G. Assanto, M. Segev, and Y. Silberberg, Discrete solitons in optics, Phys. Rep. **463**, 1 (2008).
[9] A. Szameit and S. Nolte, Discrete optics in femtosecond-laser-written photonic structures, J. Phys. B: At. Mol. Opt. Phys. **43**, 163001 (2010).
[10] D. N. Christodoulides and R. I. Joseph, Discrete self-focusing in nonlinear arrays of coupled waveguides, Opt. Lett. **13**, 794 (1988).
[11] H. S. Eisenberg, Y. Silberberg, R. Morandotti, A. R. Boyd, and J. S. Aitchison, Discrete spatial optical solitons in waveguide arrays, Phys. Rev. Lett. **81**, 3383 (1998).
[12] Y. S. Kivshar, Self-localization in arrays of defocusing waveguides Opt. Lett. **18**, 1147 (1993).
[13] A. B. Aceves, A. M. Rubenchik, S. K. Turitsyn, and C. De Angelis, Multidimensional solitons in fiber arrays, Opt. Lett. **19**, 329 (1994).
[14] E. W. Laedke, K. H. Spatschek, and S. K. Turitsyn, Stability of discrete solitons and quasicollapse to intrinsically localized modes, Phys. Rev. Lett. **73**, 1055 (1994).
[15] A. B. Aceves, G. G. Luther, C. De Angelis, A. M. Rubenchik, and S. K. Turitsyn, Energy localization in nonlinear fiber arrays: collapse-effect compressor, Phys. Rev. Lett. **75**, 73 (1995).
[16] A. B. Aceves, C. De Angelis, T. Peschel, R. Muschall, F. Lederer, S. Trillo, and S. Wabnitz, Discrete self-trapping, soliton interactions, and beam steering in nonlinear waveguide arrays, Phys. Rev. E **53**, 1172 (1996).
[17] Z. Y. Xu, Y. V. Kartashov, L. C. Crasovan, D. Mihalache, and L. Torner, Spatiotemporal discrete multicolor solitons, Phys. Rev. E **70**, 066618 (2004).
[18] D. Mihalache, D. Mazilu, F. Lederer, Y. V. Kartashov, L. C. Crasovan, and L. Torner, Stable three-dimensional spatiotemporal solitons in a two-dimensional photonic lattice, Phys. Rev. E **70**, 055603 (2004).
[19] K. G. Makris, S. Suntsov, D. N. Christodoulides, G. I. Stegeman, and A. Haché, Discrete surface solitons, Opt. Lett. **30**, 2466 (2005).
[20] N. C. Panoiu, R. M. Osgood, and B. A. Malomed, Semidiscrete composite solitons in arrays of quadratically nonlinear waveguides, Opt. Lett. **31**, 1097 (2006).
[21] D. Mihalache, D. Mazilu, F. Lederer, and Y. Kivshar, Stable discrete surface light bullets, Opt. Express **15**, 589 (2007).
[22] A. B. Aceves, O. V. Shtyrina, A. M. Rubenchik, M. P. Fedoruk, and S. K. Turitsyn, Spatiotemporal

optical bullets in two-dimensional fiber arrays and their stability, Phys. Rev. A **91**, 033810 (2015).

[23] J. W. Fleischer, M. Segev, N. K. Efremidis, and D. N. Christodoulides, Observation of two-dimensional discrete solitons in optically induced nonlinear photonic lattices, Nature (London) **422**, 147 (2003).

[24] D. Neshev, E. Ostrovskaya, Yu. Kivshar, and W. Krolikowski, Spatial solitons in optically induced gratings, Opt. Lett. **28**, 710 (2003).

[25] D. N. Neshev, T. J. Alexander, E. A. Ostrovskaya, and Yu. S. Kivshar, Observation of discrete vortex solitons in optically induced photonic lattices, Phys. Rev. Lett. **92**, 123903 (2004).

[26] S. Suntsov, K. G. Makris, D. N. Christodoulides, G. I. Stegeman, H. Haché, R. Morandotti, H. Yang, G. Salamo, and M. Sorel, Observation of discrete surface solitons, Phys. Rev. Lett. **96**, 063901 (2006).

[27] A. Szameit, Y. V. Kartashov, F. Dreisow, T. Pertsch, S. Nolte, A. Tünnermann, and L. Torner, Observation of two-dimensional surface solitons in asymmetric waveguide arrays, Phys. Rev. Lett. **98**, 173903 (2007).

[28] M. Heinrich, A. Szameit, F. Dreisov, R. Keil, S. Minardi, T. Pertsch, S. Nolte, A. Tünnermann, and F. Lederer, Observation of three-dimensional discrete-continuous X waves in photonic lattices, Phys. Rev. Lett. **103**, 113903 (2009).

[29] S. Minardi, F. Eilenberger, Y. V. Kartashov, A. Szameit, U. Röpke, J. Kobelke, K. Schuster, H. Bartelt, S. Nolte, L. Torner, F. Lederer, A. Tünnermann, and T. Pertsch, Three-dimensional light bullets in arrays of waveguides, Phys. Rev. Lett. **105**, 263901 (2010).

[30] F. Eilenberger, K. Prater, S. Minardi, R. Geiss, U. Röpke, J. Kobelke, K. Schuster, H. Bartelt, S. Nolte, A. Tünnermann, and T. Pertsch, Observation of discrete, vortex light bullets, Phys. Rev. X **3**, 041031 (2013).

[31] H. Leblond, B. A. Malomed, and D. Mihalache, Spatiotemporal vortices in fiber bundles, Phys. Rev. A **77**, 063804 (2008).

[32] H. Leblond, B. A. Malomed, and D. Mihalache, Spatiotemporal vortex solitons in hexagonal arrays of waveguides, Phys. Rev. A **83**, 063825 (2011).

[33] O. Lahav, O. Kfir, P. Sidorenko, M. Mutzafi, A. Fleisher, and O. Cohen, Three-dimensional spatiotemporal pulse-train solitons, Phys. Rev. X **7**, 041051 (2017).

[34] N. A. Veretenov, S. V. Fedorov, and N. N. Rosanov, Topological vortex and knotted dissipative optical 3D solitons generated by 2D vortex solitons, Phys. Rev. Lett. **119**, 263901 (2017).

[35] O. V. Shtyrina, M. P. Fedoruk, Y. S. Kivshar, and S. K. Turitsyn, Coexistence of collapse and stable spatiotemporal solitons in multimode fibers, Phys. Rev. A **97**, 013841 (2018).

[36] Th. Brabec and F. Krausz, Nonlinear optical pulse propagation in the single-cycle regime Phys. Rev. Lett. **78**, 3282 (1997).

[37] Sh. Amiranashvili, U. Bandelow and N. Akhmediev, Dispersion of nonlinear group velocity determines shortest envelope solitons, Phys. Rev. A **84**, 043834 (2011).

[38] A. V. Husakou and J. Herrmann, Supercontinuum generation of higher-order solitons by fission in photonic crystal fibers, Phys. Rev. Lett. **87**, 203901 (2001).

[39] Sh. Amiranashvili, U. Bandelow, and N. Akhmediev, Few-cycle optical solitary waves in nonlinear dispersive media, Phys. Rev. A **87**, 013805 (2013).

[40] E. V. Kazantseva, A. I. Maimistov, and J.-G. Caputo, Reduced Maxwell-Duffing description of extremely short pulses in nonresonant media, Phys. Rev. E **71**, 056622 (2005).

[41] N. N. Rosanov, V. V. Kozlov, and S. Wabnitz, Maxwell-Drude-Bloch dissipative few-cycle optical solitons, Phys. Rev. A **81**, 043815 (2010).

[42] S. V. Sazonov, On the nonlinear optics of few-cycle pulses, Bull. Russian Acad. Sciences **75**, 157 (2011).

[43] H. Leblond and D. Mihalache, Models of few optical cycle solitons beyond the slowly varying envelope approximation, Phys. Rep. **523**, 61 (2013).

[44] D. J. Frantzeskakis, H. Leblond, and D. Mihalache, Nonlinear optics of intense few-cycle pulses:

An overview of recent theoretical and experimental developments, Rom. J. Phys. **59**, 767 (2014).
[45] S. V. Sazonov, Optical solitons in systems of two-level atoms, Rom. Rep. Phys. **70**, 401 (2018).
[46] I. V. Mel'nikov, D. Mihalache, F. Moldoveanu, N.-C. Panoiu, Quasiadiabatic following of femtosecond optical pulses in a weakly excited semiconductor, Phys. Rev. A **56**, 1569 (1997).
[47] T. Schäfer and C. E. Wayne, Propagation of ultra-short optical pulses in cubic nonlinear media, Physica D **196**, 90 (2004).
[48] A. Sakovich and S. Sakovich, The short pulse equation is integrable, J. Phys. Soc. Jpn. **74**, 239 (2005).
[49] J. C. Brunelli, The short pulse hierarchy, J. Math. Phys. **46**, 123507 (2005).
[50] H. Leblond and F. Sanchez, Models for optical solitons in the two-cycle regime, Phys. Rev. A **67**, 013804 (2003).
[51] A. Nazarkin, Nonlinear optics of intense attosecond light pulses, Phys. Rev. Lett. **97**, 163904 (2006).
[52] H. Leblond, H. Triki, and D. Mihalache, Derivation of a generalized double sine-Gordon equation describing ultrashort soliton propagation in optical media composed of multilevel atoms, Phys. Rev. A **86**, 063825 (2012).
[53] H. Leblond, S. V. Sazonov, I. V. Mel'nikov, D. Mihalache, and F. Sanchez, Few-cycle nonlinear optics of multicomponent media, Phys. Rev. A **74**, 063815 (2006).
[54] H. Leblond and D. Mihalache, Few-optical-cycle solitons: Modified Korteweg-de Vries-sine Gordon equation versus other non-slowly varying envelope approximation models, Phys. Rev. A **79**, 063835 (2009).
[55] S. P. Popov, Numerical analysis of soliton solutions of the modified Korteweg-de Vries-sine-Gordon equation, Comput. Math. and Mathematical Phys. **55**, 437 (2015).
[56] S. V. Sazonov, Extremely short and quasi-monochromatic electromagnetic solitons in a two-component medium, JETP **92**, 361 (2001).
[57] V. G. Bespalov, S. A. Kozlov, Yu. A. Shpolyanskiy, and I. A. Walmsley, Simplified field wave equations for the nonlinear propagation of extremely short light pulses, Phys. Rev. A **66**, 013811 (2002).
[58] S. A. Skobelev, D. V. Kartashov, and A. V. Kim, Few-optical-cycle solitons and pulse self-compression in a Kerr medium, Phys. Rev. Lett. **99**, 203902 (2007).
[59] S. V. Sazonov and N. V. Ustinov, Extremely short vector solitons under the conditions of conical refraction, JETP Lett. **99**, 503 (2014).
[60] S. Amiranashvili, U. Bandelow, and N. Akhmediev, Ultrashort optical solitons in transparent nonlinear media with arbitrary dispersion, Opt. Quant. Electron. **46**, 1233 (2014).
[61] S. V. Sazonov, Few-cycle solitons in the medium with permanent dipole moment under conditions of the induced birefringence, Opt. Commun. **380**, 480 (2016).
[62] A. Hofstrand, J. V. Moloney, Modeling ultrashort electromagnetic pulses with a generalized Kadomtsev-Petviashvili equation, Physica D **366**, 51 (2018).
[63] S. V. Sazonov and N. V. Ustinov, New integrable model of propagation of the few-cycle pulses in an anisotropic microdispersed medium, Physica D **366**, 1 (2018).
[64] H. Leblond and S. Terniche, Waveguide coupling in the few-cycle regime, Phys. Rev. A **93**, 043839 (2016).
[65] S. Terniche, H. Leblond, D. Mihalache, and A. Kellou, Few-cycle optical solitons in linearly coupled waveguides, Phys. Rev. A. **94**, 063836 (2016).
[66] H. Leblond, D. Kremer, and D. Mihalache, Few-cycle spatiotemporal optical solitons in waveguide arrays, Phys. Rev. A. **95**, 043839 (2017).
[67] H. Leblond, The reductive perturbation method and some of its applications, J. Phys. B: At. Mol. Opt. Phys. **41**, 043001 (2008).
[68] T. B. Benjamin and J. E. Feir, The desintegration of wave trains in deep water. Part 1. Theory, J. Fluid. Mech. **27**, 417 (1967).
[69] J. T. Stuart and R. C. DiPrima, The Eckhaus and Benjamin-Feir resonance mechanisms, Proc. R.

Soc. Lond. A **362**, 27 (1978).